Elsevier Editorial System(tm) for Journal of the European Ceramic Society

Manuscript Draft

Manuscript Number:

Title: Exceptional micromachining performance of silicon carbide ceramics by adding graphene nanoplatelets

Article Type: SI: WGCC 2016

Keywords: graphene; silicon carbide; ceramic matrix composites; machining; microcomponents

Corresponding Author: Dr. Manuel Belmonte,

Corresponding Author's Institution: Institute of Ceramics and Glass (CSIC)

First Author: Florian Zeller

Order of Authors: Florian Zeller; Claas Müller; Pilar Miranzo; Manuel Belmonte

Abstract: The electrical discharge machining (EDM) performance of silicon carbide (SiC) ceramics is investigated varying their electrical and thermal conductivities by introducing graphene-based fillers. SiC/graphene nanocomposites with different amounts and types of graphene are manufactured. As graphene flakes appear preferred oriented within the material, the nanocomposites are EDMed in orthogonal directions respecting the graphene basal plane. The addition of graphene nanoplatelets to SiC ceramics dramatically increases the material removal rate (MRR), as compared to monolithic SiC ceramics, allowing the machining of microparts with a fine dimensional precision. A relationship between the EDM response and the transport properties is established, with a strong and direct dependence of MRR with the electrical conductivity of the workpieces, i.e., with the graphene content; while an inverse dependence with the thermal conductivity is observed. The EDM testing orientation of the nanocomposites clearly influences the EDM performance for graphene contents below the electrical percolation threshold.

Suggested Reviewers: Erica Corral
The University of Arizona, USA
elcorral@email.arizona.edu
Expert on structural ceramics and composites

Young-Wook Kim
The University of Seoul, Republic of Korea
ywkim@uos.ac.kr
Expert on EDM of ceramics

Myung-Chang Kan
Pusan National University, South Korea
kangmc@pusan.ac.kr
Expert on EDM of ceramics

Exceptional micromachining performance of silicon carbide ceramics by adding graphene nanoplatelets

Florian Zeller[1], Claas Müller[1], Pilar Miranzo[2], Manuel Belmonte[2*]

[1]Laboratory for Process Technology, Department of Microsystems Engineering - IMTEK, University of Freiburg, Georges-Köhler-Allee 103, 79110 Freiburg, Germany

[2]Institute of Ceramics and Glass (ICV-CSIC), Kelsen 5, 28049 Madrid, Spain

Abstract

The electrical discharge machining (EDM) performance of silicon carbide (SiC) ceramics is investigated varying their electrical and thermal conductivities by introducing graphene-based fillers. SiC/graphene nanocomposites with different amounts and types of graphene are manufactured. As graphene flakes appear preferred oriented within the material, the nanocomposites are EDMed in orthogonal directions respecting the graphene basal plane. The addition of graphene nanoplatelets to SiC ceramics dramatically increases the material removal rate (MRR), as compared to monolithic SiC ceramics, allowing the machining of microparts with a fine dimensional precision. A relationship between the EDM response and the transport properties is established, with a strong and direct dependence of MRR with the electrical conductivity of the workpieces, i.e., with the graphene content; while an inverse dependence with the thermal conductivity is observed. The EDM testing orientation of

*Corresponding author. Phone: +34-917355863; Fax: +34-917355843. E-mail: mbelmonte@icv.csic.es (M. Belmonte)

the nanocomposites clearly influences the EDM performance for graphene contents below the electrical percolation threshold.

Keywords: graphene; silicon carbide; ceramic matrix composites; machining; microcomponents

1. Introduction

The development of silicon carbide (SiC) ceramic microcomponents to be used, among others, as part of microturbines, microreactors, and microelectromechanical systems or as catalytic microsupports is attracting a great interest mainly due to the excellent thermal, tribological and mechanical performance at high temperature of these ceramics, jointly with their good resistance to corrosive and harsh environments [1,2]. However, the machining of SiC complex microparts is a complicated task when using diamond grinding wheels, the most common technique, due to the high hardness and brittle nature of SiC, which leads to expensive and time consuming processes for getting microcomponents with relatively low accuracy and surface finishing.

Electrical discharge machining (EDM) arises as one of the most suitable methods to overcome these difficulties, since the material removal is caused by electrical discharges, and mechanical forces between the electrode and the workpiece are not developed [3].The main constraint for EDM is that a minimum electrical conductivity (σ_e) of the workpiece is required (> 0.3-1.0 $S \cdot m^{-1}$) to enable the electrical discharges [4], which can be a clear limitation in the machining process of SiC ceramics

typically exhibiting lower conductivity values than those needed. Different approaches have been considered to enhance the discharge efficiency of ceramics. In this way, Fukuzawa et al. [5] proposed the use of an assisting electrode method (AEM) to machine insulator ceramics by coating the workpiece with a conductive layer. This layer promotes the first discharges between the electrode and the workpiece. The pyrolytic carbon generated during the decomposition of the oil-based dielectric fluid adheres to the ceramic surface, leading to the continuous formation of an intrinsic conductive layer on the workpiece that allows the EDM process. Although AEM has successfully been employed for non-conductive SiC ceramics [6,7], the material removal rate was low and the electrode wear rate was quite high. Another approach to promote the EDM of low electrical conductive materials consisted in the addition of conductive powders into the dielectric fluid, known as powder mixed EDM (PMEDM) process [8]. Liew et al. [9] improved the electrical discharge frequency and the EDM performance of reaction bonded-SiC (RB-SiC) ceramics by incorporating electrical conductor carbon nanofibers to the dielectric fluid. Finally, successful EDM attempts were carried out in electrically conducting SiC materials. This is the case of the previously mentioned RB-SiC ceramics [10], where the silicon remained after the infiltration process slightly increased σ_e up to ~ 10 $S \cdot m^{-1}$, or more noticeably by adding yttrium nitrate as sintering additive into SiC matrix to achieve σ_e values of ~ 10^4 $S \cdot m^{-1}$ that allowed the EDM of quite complex SiC shapes [11].

During the last years, graphene, in the form of graphene nanoplatelets (GNPs) or graphene oxide (GO) sheets, has become an extraordinary filler to enhance the electrical response of low conductor ceramics such as Al_2O_3 [12], ZrO_2 [13], Si_3N_4 [14] or B_4C [15]. Some of the present authors were also able to increase the electrical conductivity

of SiC ceramics in three orders of magnitude by introducing GNPs [16], which, at the same time, extraordinarily improved the tribological [17] and mechanical [18] responses of these materials. Therefore, ceramic/graphene composites could be promising materials to be EDMed, augmenting the machining efficiency as well. In this way, few works have recently reported a better EDM performance of Si_3N_4 [19], B_4C [15], and Al_2O_3 [20] by introducing GNPs fillers into the ceramic matrices. However, to the best of our knowledge, EDM has not been employed to manufacture SiC/graphene parts hitherto.

In the present work, EDM tests were carried out in three different SiC monoliths and two SiC/GNPs nanocomposites with distinct GNPs contents. All these materials scanned a wide range of properties, especially in terms of the electrical and thermal conductivities, aiming to establish a relationship between the EDM response and the transport properties. Besides, the machining experiments were conducted varying the energy conditions, and the graphene-based nanocomposites were tested on orthogonal surfaces according to their anisotropic microstructure.

2. Experimental procedure

2.1. Materials fabrication. Five different SiC-based materials were chosen to explore their EDM performances (Table 1), in particular, three monolithic SiC ceramics showing distinct properties and two SiC/GNPs nanocomposites containing 10 and 20 vol.% of GNPs. Specimens of one of the monolithic SiC ceramics were commercially manufactured (CD110 grade, CeramTec, Germany); whereas for the rest of compositions fully dense specimens were produced in-house according to the

experimental procedure described elsewhere [16,21]. In brief, SiC/GNPs powders were processed by mixing and sonicating two isopropyl alcohol suspensions independently prepared: one containing commercial GNPs (type N006, Angstron Materials Inc., USA) that were dispersed through a sonication process; and another SiC-based suspension consisting on the attrition milled ceramic powder composition - 93 wt.% of micro-sized β-SiC (BF-17A, H.C. Starck, Germany), 5 wt.% of Y_2O_3(Grade C,H.C. Starck, Germany), and 2 wt.% of Al_2O_3 (SM8, Baikowski Chimie, France). The dried and sieved SiC/GNPs powder mixtures (labelled as 10GNPs and 20GNPs for 10 and 20 vol.% GNPs contents, respectively) were then spark plasma sintered (SPS, Dr. Sinter, SPS-510CE, Japan) into disc specimens of 20 mm × 3 mm at 1800 ºC for 5 min, applying a uniaxial pressure of 50 MPa during the heating cycle, and using a vacuum atmosphere of ~6 Pa. Monolithic SiC specimens (0 vol.% GNPs) were equally processed from the ceramic powders. Micro-sized and nano-sized β-SiC (NanoAmor, USA) were employed as SiC raw powder into the monolithic ceramic composition. Accordingly, the manufactured monolithic SiC specimens were labelled as μ-SiC and n-SiC, respectively; meanwhile the commercial one was identified as C-SiC. Table 1 collects the different materials and their main properties.

Table 1. Materials selected for EDM tests and their main morphological characteristics and properties [16,18,21,22]: mean particle size (d_{50}), flexural strength (σ_f), fracture toughness (K_{IC}), electrical conductivity (σ_e), and thermal conductivity (k_T). Transport data (σ_e and k_T) in the parallel (||) and perpendicular (⊥) directions to the SPS pressing axis are also included for some materials. †Data reported by the supplier. *K_{IC} value

estimated by Vickers indentations at 49 N. For the rest of materials K_{IC} was assessed by the surface crack in flexure method.

Material	**Label**	**d_{50} (μm)**	**σ_f (MPa)**	**K_{IC} (MPa $m^{1/2}$)**	**σ_e (S·m^{-1})**	**k_T (W·m^{-1}·K^{-1})**
Commercial monolithic SiC	C-SiC	3-5†	440†	3.8†	2 x 10^{-6}†	100†
Monolithic Nano SiC	n-SiC	0.4	---	3.5*	~33	29 (‖) 67 (⊥)
Monolithic Micro SiC	μ-SiC	0.6	373	3.2	1 (‖) 5 (⊥)	43 (‖) 65 (⊥)
Micro SiC/10 vol.%GNPs	10GNPs	0.6	602	5.9	158 (‖) 922 (⊥)	33 (‖) 73 (⊥)
Micro SiC/20 vol.%GNPs	20GNPs	0.7	401	4.1	919 (‖) 4380 (⊥)	25 (‖) 84 (⊥)

It is important to remark that μ-SiC and n-SiC ceramics contained ~3-4 vol.% of graphene multilayers, which were in-situ grown at the SiC grain boundaries during the SPS process [21]. Besides, both types of graphene fillers, the in-situ grown and the added GNPs, appeared into the material preferentially oriented with their basal (ab)

plane perpendicular to the SPS pressing axis [16] (see an example in Figure 1a), leading to materials with anisotropic properties (Table 1).

2.2. EDM tests. The EDM trials were performed using a SARIX micro-EDM machine (Model SX-200-HPM, Switzerland). In the case of n-SiC ceramics and 10GNPs and 20GNPs nanocomposites, their σ_e values (Table 1) were well above the limit ($\geq 1\ S \cdot m^{-1}$) for directly using the EDM process. However, for the low electrical conducting C-SiC and µ-SiC monolithic ceramics, it was not possible to employ EDM and AEM was required to enable the machining process. In this way, C-SiC and µ-SiC specimens were coated by screen printing with a conductive carbon lacquer layer of ~ 25 µm of thickness.

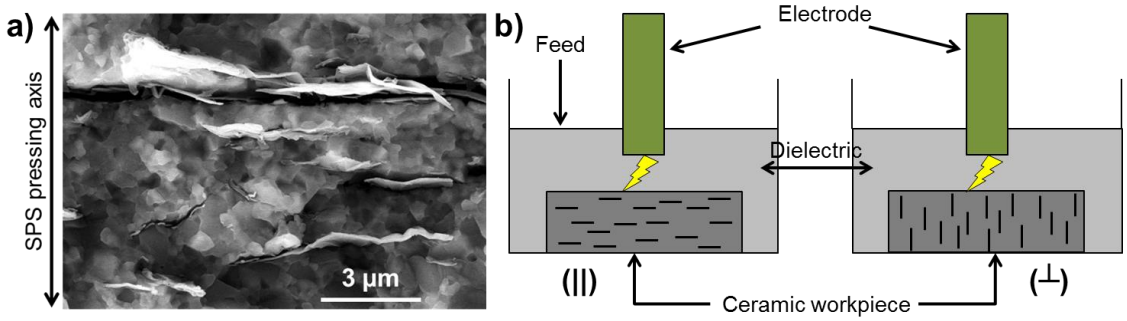

Figure 1. a) SEM micrograph of the fracture surface of 10GNPs composite showing the preferential orientation of the GNPs with their basal plane perpendicular to the SPS pressing axis. b) Scheme of the EDM tests performed on the parallel (||) and perpendicular (⊥) directions of the materials with respect to the SPS pressing axis.

To explore the EDM performance of the ceramics and nanocomposites, three different EDM energy conditions were selected (Table 2) from preliminary trials that enabled a stable EDM process in all materials. In particular, the selected energy settings

corresponded to conventional fine machining (EDM-F) and rough and fast machining (EDM-R1 and EDM-R2) processes. In the case of EDM-R1 and EDM-R2, the generator only allows one discharge per pulse width, while for EDM-F a larger number of discharges having shorter on times takes place. The main difference between rough conditions is that the applied voltage is higher for EDM-R2 (Table 2). A tungsten carbide rod with a diameter of 300 µm was used as tool electrode and microgrooves were machined into the materials with the rotating microrods. The tests were carried out using a machining depth and length of 50 µm and 200 µm, respectively, and an infeed of 10 µm. IME 110 (Oelheld GmbH, Germany) was used as dielectric fluid. All the materials were EDMed in the (||) direction (Fig. 1b). In addition, EDM tests were also carried out in the (⊥) direction (Fig. 1b) for the materials presenting a clear anisotropy on their electrical and thermal conductivities (Table 2).

The material removal rate (MRR) was calculated using the process time and the removed volume optically measured with a coordinate measuring machine (Werth Videocheck HA400, Germany). The surface roughness (S_q) of the machined surface was optically measured with a white light interferometer (Zygo, USA). The electrode tool wear ratio (EWR) was assessed from the ratio between the electrode wear volume and the removed workpiece volume. The analysis of the machined surfaces was done by scanning electron microscopy (SEM, DSM 962, Zeiss, Germany) and micro-Raman spectroscopy (Alpha300 WITec GmbH, Germany) using the 532 nm laser wave-length excitation. Raman maps of 25 × 25 pixels, recording one spectrum per pixel and using 1 s of acquisition time, were acquired on 50 × 50 μm^2 scanned areas. The micro hardness (H) of some of the materials was determined on the unmachined and EDMed surfaces at room-temperature (MHT-10, Anton Paar-Paar Physica, USA) using a diamond indenter

and an indentation force of 2.9 N. At least 10 indentation tests were carried out per material.

Table 2. Parameters of the different fine (EDM-F) and rough (EDM-R) machining conditions.

Energy conditions	**Voltage (V)**	**Current (index)**	**Frequency (kHz)**	**Pulse width (µs)**
EDM-F	200	1	100	1
EDM-R1	140	25	100	1
EDM-R2	200	25	100	1

3. Results and discussion

The EDM performance of the different tested materials, machined in the (||) direction, versus the energy conditions is collected in Figure 2. At first glance, the addition of GNPs to SiC ceramics dramatically increased the MRR (Fig. 2a), ranging, for EDM-F testing condition, from 0.37 $x10^{-2}$ $mm^3 \cdot min^{-1}$ (C-SiC) to 1.05 $x10^{-2}$ $mm^3 \cdot min^{-1}$ (20GNPs), which represents an augment in MRR of ~186%. This outstanding increment could be explained by the electrical and thermal properties of the EDMed materials. As it is shown in Table 1, σ_e considerably augments in the (||) direction while k_T moderately decreases, both when compared with monolithics having similar matrices characteristics. In general, a high electrical conducting workpiece would enlarge the probability for producing successful discharges during the EDM

process, increasing the material removal. Actually, Figure 3a shows a strong and direct increasing dependence of MRR with σ_e (for values above 1 $S \cdot m^{-1}$), i.e., with the GNPs content in the case of the nanocomposites. In addition, comparing the MRR response of the different monolithic SiC, the best performance was attained for n-SiC ceramics, which exhibits the highest electrical conductivity (Table 1) due to both the graphene-like network formed in-situ and the strong doping during its sintering [21,23].

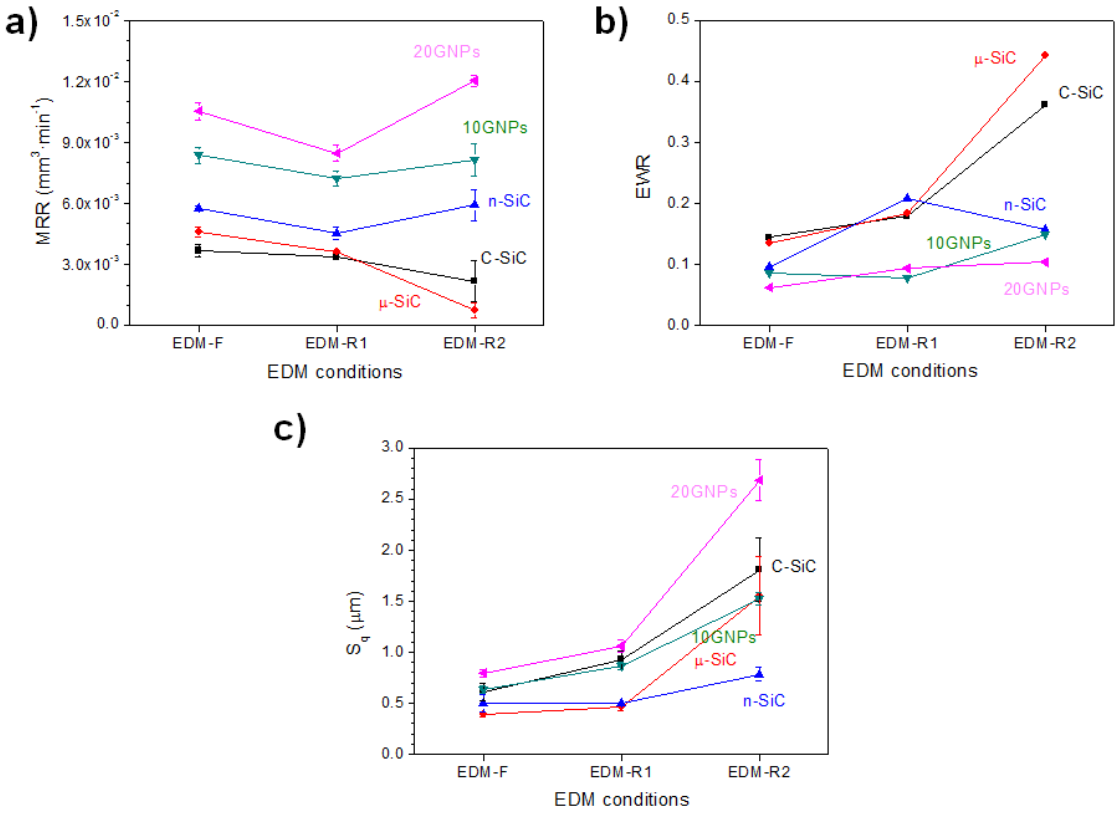

Figure 2. a) Material removal rate (MRR), b) electrode wear rate (EWR), and c) surface roughness (S_q) as a function of the EDM conditions for the different ceramic materials machined in the (||) configuration.

The thermal conductivity of the workpiece also influences the EDM process by affecting the dissipation of the generated heat and the material removal by thermal spalling. In this way, MRR data exhibited an inverse dependence with k_T (Fig. 3b). Besides, as k_T decreases (GNPs nanocomposites), heat losses diminish and the energy process is much focused to melt the workpiece, improving the EDM performance. Therefore, the better machining response of GNPs nanocomposites is explained by the combined effect of an increasing electrical conductivity and decreasing thermal conductivity.

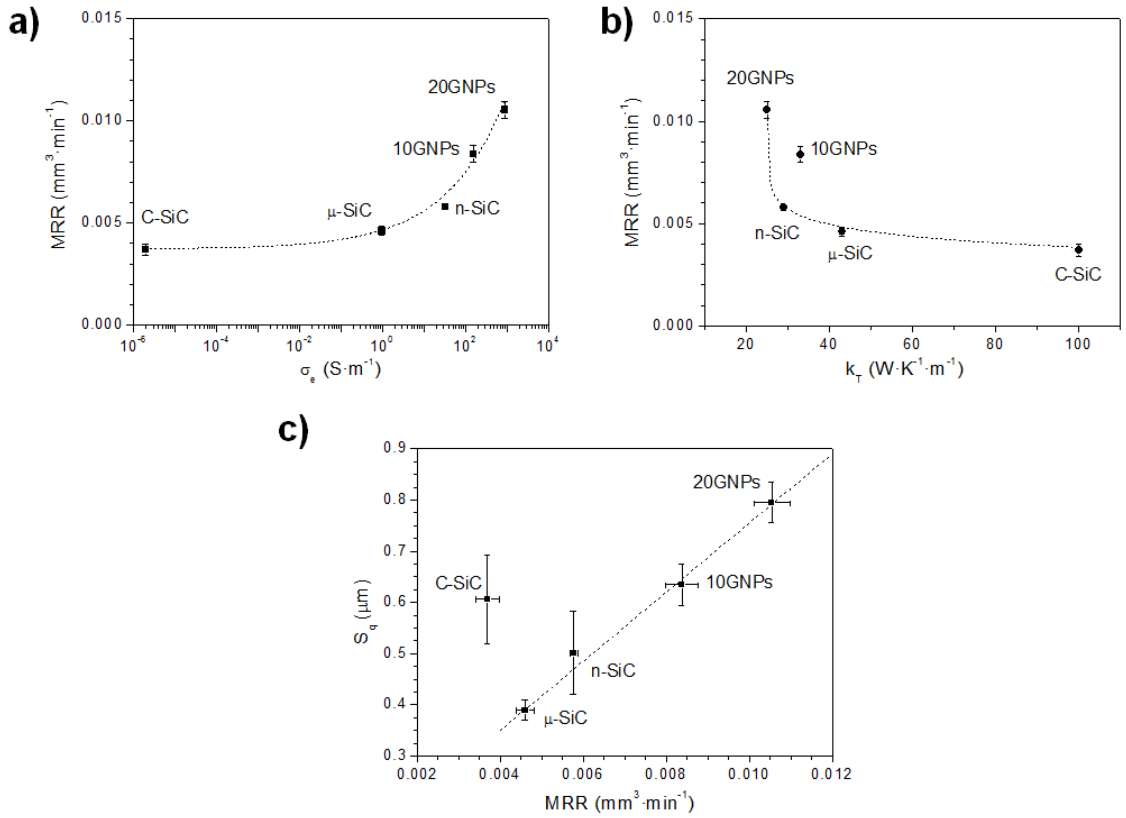

Figure 3. a) Material removal rate (MRR) at EDM-F as a function of the electrical and b) thermal conductivities of the EDMed materials in the (||) configuration. (c) Surface roughness (S_q) evolution versus material removal rate (MRR) using EDM-F settings and (||) configuration.

At a first glance, the effect of the machining energy parameters on MRR does not follow a clear trend (Fig. 2a). Initially, larger MRR values should be expected for rough machining EDM-R1 and EDM-R2 settings. This is not the case for EDM-R1, where MRR decreased for all the materials probably due to both the lower spark voltage and the limitation of one discharge per pulse width, in comparison with higher voltage and the larger number of discharges for EDM-F. Despite the discharges limitation of EDM-R2, its higher voltage augmented MRR for the materials machined using EDM (n-SiC, 10GNPs, 20GNPs) up to similar or even higher values than those attained for EDM-F. However, when AEM testing C-SiC and μ-SiC materials, MRR further decreased due to the excessive generation of pyrolytic carbon which was not sufficiently flushed away, causing instabilities in the machining process.

EWR for all the materials is plotted as a function of the machining conditions in Fig. 2b. The results evidence that, independently of the EDM conditions, GNPs nanocomposites led to lower EWR values (< 0.15), which is a clear indicator of their finer dimensional precision and better EDM performance. In particular, 20GNPs nanocomposite reached at EDM-F an EWR value of up to 132% and 55% lower than monolithic SiC ceramics machined with and without AEM, respectively. Besides, a larger GNPs content provided a better EWR response (37% at EDM-F for 20 vol.% of GNPs). In general, EWR significantly augmented for non-conducting materials as the energy parameters increased, reaching values above 0.4.

The surface analysis by SEM of the machined workpieces (Figure 4) evidenced the formation of either discharge craters in the case of AEMed materials (C-SiC and μ-

SiC, Figs. 4a,c) or a recast layer over the machined surface for the rest of conducting materials (n-SiC and GNPs nanocomposites, Figs. 4b,d,e), the latter confirming a removal mechanism by melting process of the liquid-phase sintered materials.

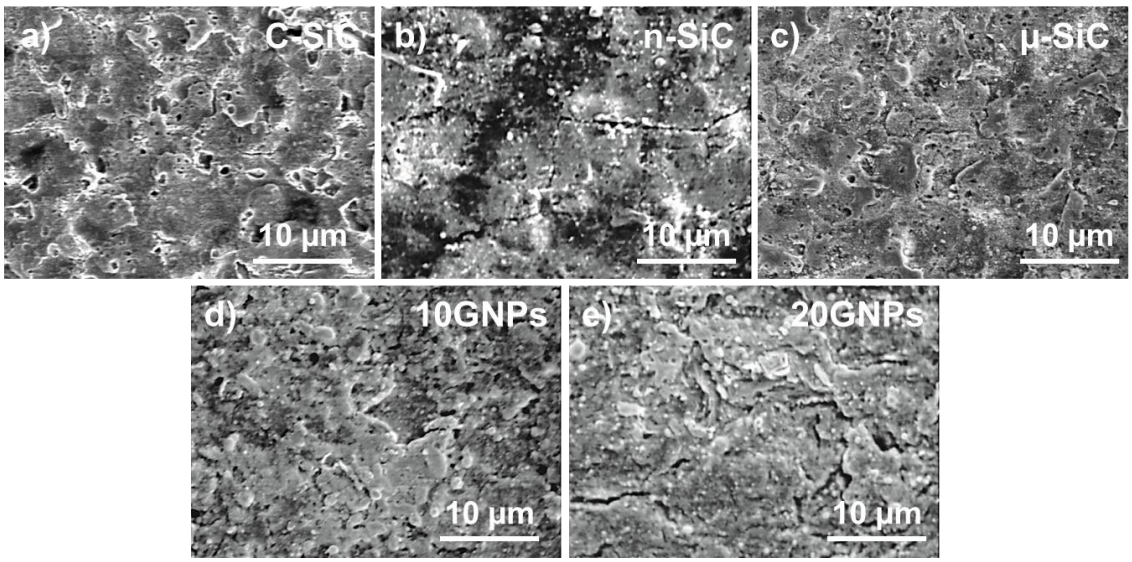

Figure 4. SEM micrographs of the EDMed surfaces at EDM-F in the (||) configuration for: a) C-SiC, b) n-SiC, c) µ-SiC, d) 10GNPs, and e) 20GNPs materials.

An important issue in the EDM process is the surface roughness of the machined workpieces, which must be low enough to avoid further polishing treatments that would raise the final production costs. As expected, the fine machining setting conditions (EDM-F) produced S_q values below 1 µm for all materials (Fig. 2c); whereas S_q increased for rough machining conditions, especially for EDM-R2 (up to 2.7 µm for 20GNPs nanocomposite), where an increase of the energy input into the surface occurred. In addition, when plotting S_q versus MRR at EDM-F, a clear relationship was observed (Fig. 3c). In this way, the roughness of the machined workpieces linearly augmented with the MRR except for C-SiC. The unexpected high S_q attained for this

ceramic material considering its relatively low MRR could be explained by its large grain size (3-5 μm), almost one order of magnitude bigger than for the rest of materials (Table 1), that would produce deeper craters and, hence, higher S_q. In view of EDM-F led to the best EDM performance of the tested materials in terms of high MMR, and low EWR and S_q, this energy parameter was selected for the following studies.

Micro-Raman spectroscopy can also be used as tool to analyse the surface damage of the EDMed surfaces. In this way, n-SiC ceramics and 10GNPs and 20GNPs nanocomposites, chosen by their better EDM performance, were characterized by Raman spectroscopy (Figure 5). The unmachined surfaces (Fig. 5a) of the GNPs nanocomposites exhibited Raman peaks centred at ~805 cm^{-1} and ~975 cm^{-1}, corresponding to the transverse-optical (TO) and longitudinal optical (LO) modes of β-SiC [24], respectively, and the three characteristic bands of graphitic species associated to GNPs [25], i.e., D- (~1360 cm^{-1}), G- (~1595 cm^{-1}), and 2D-bands (~2717 cm^{-1}). The n-SiC ceramics also present these bands, although less intense, due to the in-situ growth of a graphene network during the ceramic densification by SPS [21], and only the SiC-TO band at ~805 cm^{-1} is observed for this material reflecting its high doping level [23]. After the EDM tests (Fig. 5b), the SiC signal in all materials almost disappeared, whereas a new peak at ~520 cm^{-1} associated to silicon (Si) was detected which infers the decomposition of SiC due to the high local temperatures reached during the machining processes. Regarding the GNPs, the EDMed surfaces showed the same characteristic bands than the untested ones, although their intensity ratios substantially varied. As it can be seen in Fig. 5c, the intensity ratio between D and G-bands (I_D/I_G), commonly employed as tool to estimate the crystallinity (or defective) degree of the graphene species, dramatically increased after the EDM process in all materials, from

0.95 to 1.37 for n-SiC, 0.26 to 1.22 for 10GNPs, and 0.36 to 0.92 for 20GNPs. These results mean that graphene flakes on the machined surface became highly damaged after the severe testing conditions used for EDM.

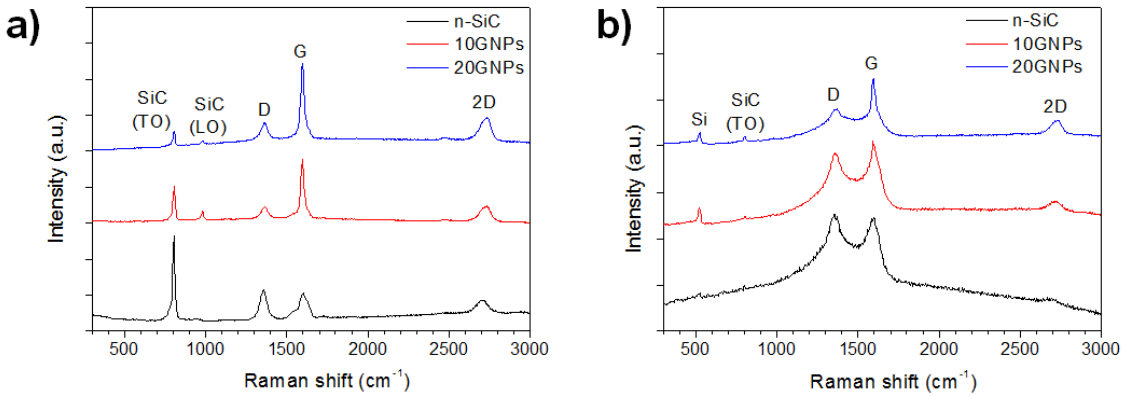

c)

I_D/I_G	Unmachined	EDMed
n-SiC	0.95	1.37
10GNPs	0.26	1.22
20GNPs	0.36	0.92

Figure 5. Average Raman spectra of the n-SiC ceramics and 10GNPs and 20GNPs nanocomposites before (a) and after (b) EDM tests performed at EDM-F in the (||) configuration. c) Table summarizing the Raman I_D/I_G values for the unmachined and EDMed surfaces.

As it was previously reported by some of the authors [17], the addition of GNPs to SiC decreased the hardness due to the sliding phenomenon of the graphene layers within the nanoplatelets. After EDM, the surface damage of the machined workpiece, evidenced by the decomposition of SiC, and in the case of nanocomposites by the GNPs degradation as well, led to the reduction of the hardness. After EDM process, H values

for both nanocomposites were very similar, which means that hardness is controlled by the recast layer.

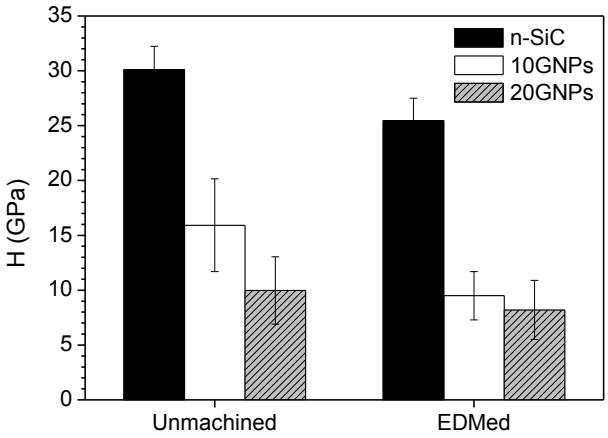

Figure 6. Hardness (H) tested in the (||) direction for the unmachined and EDMed (EDM-F) surfaces for n-SiC, 10GNPs, and 20GNPs materials.

As a proof of concept of the excellent EDM performance attained for GNPs nanocomposites in absence of the AEM, different high quality micropillars and microholes were machined (Figure 7). The EDMed structures showed in all cases very sharp and defined edges with no sign of damage, proving the benefits of adding graphene fillers to low electrically conducting ceramics for EDM microfeatures with high structural stability.

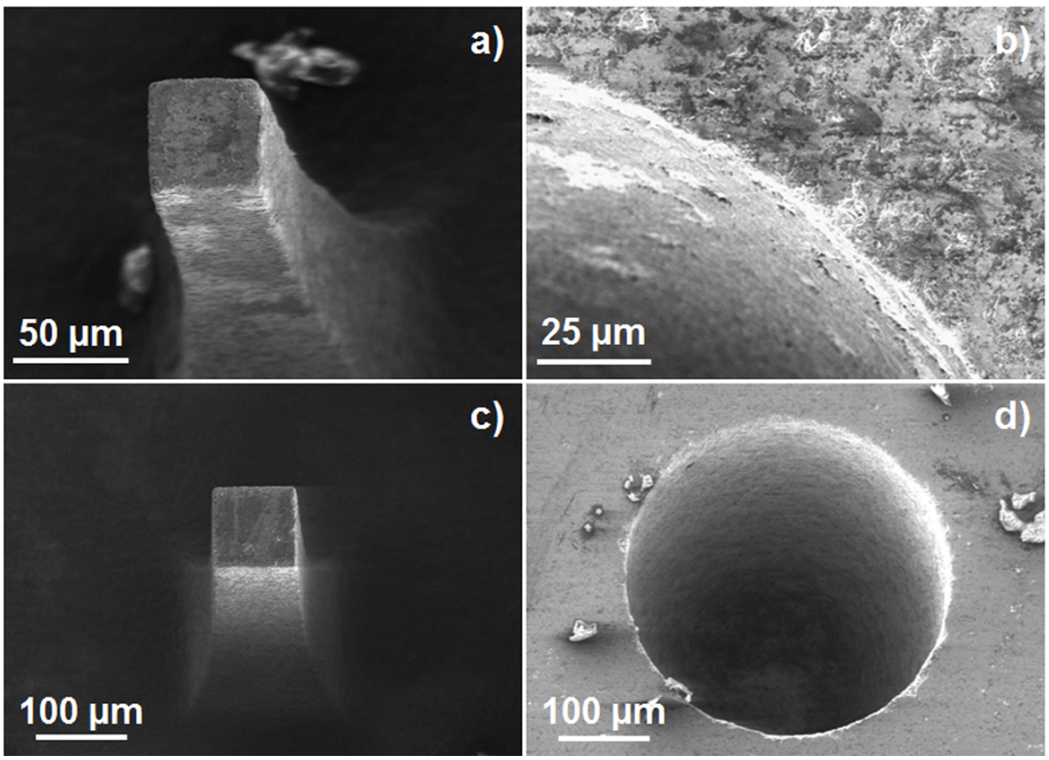

Figure 7. SEM micrographs showing some examples of EDMed features (micropillar and microhole) in the 10GNPs (a,b) and 20GNPs nanocomposites (c,d). High magnification SEM image in b) shows the edge of a microhole.

The EDM performance in the (⊥) configuration for n-SiC ceramics and GNPs nanocomposites is depicted in Figure 8, where the fine machining conditions (EDM-F) seem to get the best MRR response (Fig. 8a). Interestingly, when comparing MRR for both testing directions at EDM-F (Fig. 8b), similar results were attained except for the 10GNPs nanocomposite, where a 35% increase was achieved in the (⊥) direction (MRR ~ 1.1 x 10^{-2} $mm^3 \cdot min^{-1}$) as compared to data assessed in the (||) one. This behaviour is explained considering the relationship between the electrical properties and the MRR (Fig. 8c). Actually, 10GNPs shows complete connectivity between the nanoplatelets in

the (⊥) orientation (σ_e = 922 S·m^{-1}) but not in the (||) one (σ_e = 158 S·m^{-1}). Therefore, an increase in σ_e promoted more efficient electrical discharge and removal mechanisms until the electrical percolation threshold was reached, where the maximum efficiency of the EDM occurred (Fig. 8c). A further increment in σ_e above ~ 900 S·m^{-1} had a negligible effect in MRR.

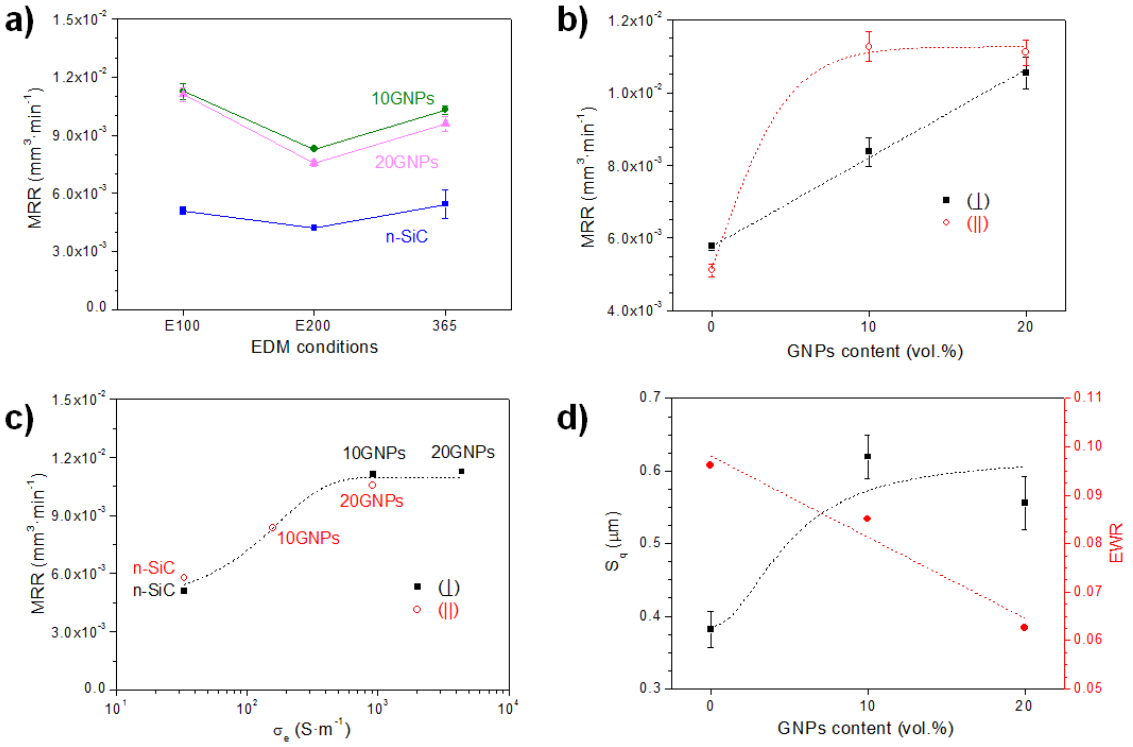

Figure 8. EDM performance of n-SiC ceramics and 10GNPs and 20GNPs nanocomposites tested in the (⊥) configuration. a) Material removal rate (MRR) versus EDM conditions, b) MRR as a function of the GNPs content for the (⊥) and (||) directions at EDM-F, c) relationship between the electrical (σ_e) conductivity and the MRR response using EDM-F settings for both testing directions, and d) surface roughness (S_q) and electrode wear rate (EWR) versus GNPs content at EDM-F in the (⊥) configuration.

As it was also observed for the (||) orientation, S_q scaled with MRR showing a similar trend (Fig. 8d), although the surface finishing kept quite smooth (< 0.7 μm) for all materials. Finally, the clear benefits of adding GNPs into EWR are shown in Fig. 8d, where an almost linear improvement of the dimensional precision (lower EWR) with the GNPs content was evidenced.

The SEM observations of the surfaces EDMed in the (⊥) direction showed the formation of a recast layer (Figure 9), as occurred for the (||) surfaces. GNPs perpendicularly oriented to the SPS pressing axis were perceived for this orientation (pointed by arrows in Figs. 9b,c).

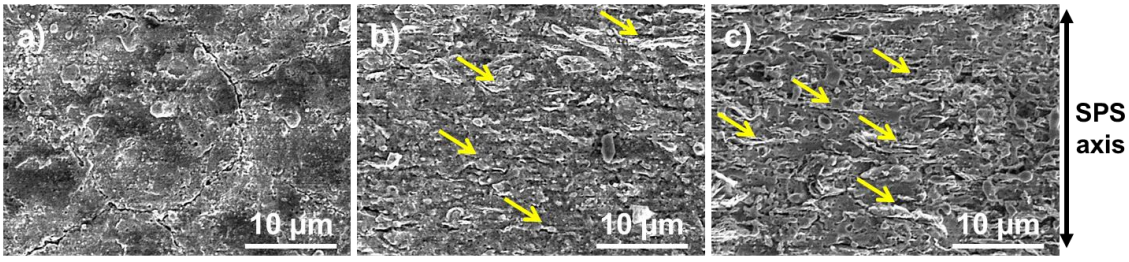

Figure 9. SEM micrographs of the EDMed surfaces at EDM-F in the (⊥) configuration for: a) n-SiC, b) 10GNPs, and c) 20GNPs materials. The arrows in (b) and (c) point the GNPs.

It can be concluded that the testing orientation has a limited influence in the EDM performance of materials with low (n-SiC) and high (20GNPs) amounts of GNPs, but it is extremely important for intermediate contents (10GNPs), the EDM response being much better for the (⊥) direction and closer to that of 20GNPs.

Conclusions

The EDM performance of SiC ceramics is clearly enhanced by adding graphene fillers to the ceramic matrix, allowing to machine microfeatures with high level of accuracy and surface roughness below 1 μm. A relationship between this outstanding EDM response of SiC/GNPs nanocomposites and the transport properties is established, showing a strong and direct dependence of MRR with the electrical conductivity of all materials. The nanocomposite with the highest GNPs content (20 vol.%) exhibits, as compared to monolithic SiC ceramics, an increment on MRR of up to 186% jointly with a reduction on EWR of up to 132%. The machining orientation affects the EDM performance of GNPs nanocomposites for intermediate contents where the electrical percolation is attained only in the direction perpendicular to the SPS pressing axis. The employ of EDM on SiC/graphene materials opens new opportunities for manufacturing complex SiC-based microcomponents to be used, among others, in the electronic and energy fields.

Acknowledgements

This work was supported by the Spanish Government (MAT2012-32944 and MAT2015-67437-R projects).

References

[1] G. Roewer, U. Herzog, K. Trommer, E. Müller, S. Frühauf, Silicon carbide-a survey of synthetic approaches, properties and applications, High Perform. non-oxide ceram.: I Struct. Bond. 101 (2002) 59-135.

[2] K. A. Schwetz, Silicon carbide based hard materials, Handbook of Ceramic Hard Materials. Wiley Online Library, Weinhein, 2008.

[3] K. H Ho, S. T Newman, State of the art electrical discharge machining (EDM), Int. J. Mach. Tool. Manu. 43 (13) (2003) 1287-1300.

[4] W. König, D. F. Dauw, G. Levy, U. Panten, EDM-Future Steps towards the Machining of Ceramics, CIRP Ann.-Manuf. Techn. 37 (2) (1998) 623-631.

[5] Y. Fukuzawa, T. Tani, E. Iwane, N. Mohri, A new machining method for insulating ceramics with an electrical discharge phenomenon, J. Ceram. Soc. Japan 103 (1995) 987-992.

[6] Y. Fukuzawa, N. Mohri, T. Tani, Electrical discharge machining method of insulating ceramics, J. Japan Soc. Precision Eng. 71 (5) (2005) 541-544.

[7] F. Zeller, T. Hösel, C. Müller, H. Reinecke, Microstructuring of non-conductive silicon carbide by electrical discharge machining, Microsyst. Technol. 20 (10-11) (2014) 1875-1880.

[8] R. Bajaj, A. K. Tiwari, A. R. Dixit, Current trends in electric discharge machining using micro and nano powder materials- A Review, Mater. Today Proc. 2 (4-5) (2015) 3302-3307.

[9] P. J. Liew, J. Yan, T. Kuriyagawa, Carbon nanofiber assisted micro electro discharge machining of reaction-bonded silicon carbide, J. Mater. Proc. Technol. 213 (7) (2013) 1076-1087.

[10] S. Clijsters, K. Liu, D. Reynaerts, B. Lauwers, EDM technology and strategy development for the manufacturing of complex parts in SiSiC, J. Mater. Proc. Technol. 210 (4) (2010) 631-641.

[11] Y.-W. Kim, K. J. Kim, H. C. Kim, N.-H. Cho, K.-Y. Lim, Electrodischarge-machinable silicon carbide ceramics sintered with yttrium nitrate, J. Am. Ceram. Soc. 94 (4) (2011) 991-993.

[12] Y. Fan, L. Wang, J. Li, J. Li, S. Sun, F. Chen, l. Chen, W. Jiang, Preparation and electrical properties of graphene nanosheet/Al_2O_3 composites, Carbon 48 (6) (2010) 1743-1749.

[13] J.-H. Shin, S.-H. Hong, Fabrication and properties of reduced graphene oxide reinforced yttria-stabilized zirconia composite ceramics, J. Eur. Ceram. Soc. 34 (5) (2014) 1297-1302.

[14] C. Ramírez, S. M. Vega-Díaz, A. Morelos-Gómez, F. M. Figueiredo, M. Terrones, M. I. Osendi, M. Belmonte, P. Miranzo, Synthesis of conducting graphene/Si_3N_4 composites by spark plasma sintering, Carbon 57 (2013) 425-432.

[15] Y. Tan, H. Luo, H. Zhang, S. Peng, Graphene nanoplatelet reinforced boron carbide composites with high electrical and thermal conductivity, J. Eur. Ceram. Soc. 36 (11) (2016) 2679-2687.

[16] B. Román-Manso, E. Domingues, F. M. Figueiredo, M. Belmonte, P. Miranzo, Enhanced electrical conductivity of silicon carbide ceramics by addition of graphene nanoplatelets, J. Eur. Ceram. Soc. 35 (10) (2015) 2723-2731.

[17] J. Llorente, B. Román-Manso, P. Miranzo, M. Belmonte, Tribological performance under dry sliding conditions of graphene/silicon carbide composites, J. Eur. Ceram. Soc. 36 (3) (2016) 429-435.

[18] M. Belmonte, A. Nistal, P. Boutbien, B. Román-Manso, M. I. Osendi, P. Miranzo, Toughened and strengthened silicon carbide ceramics by adding graphene-based fillers, Scripta Mater. 113 (2016) 127-130.

[19] D. Hanaoka, Y. Fukuzawa, C. Ramirez, P. Miranzo, M.I. Osendi, M. Belmonte, Electrical discharge machining of ceramic/carbon nanostructure composites, Procedia CIRP 6 (2013) 95-100.

[20] J.-W. Sung, K.-H. Kim, M.-C. Kang, Effects of graphene nanoplatelet contents on material and machining properties of GNP-dispersed Al_2O_3 ceramics for micro-electric discharge machining, Int. J. Precision Eng. Manufact-Green Technol. 3 (3) (2016) 247-252.

[21] P. Miranzo, C. Ramirez, B. Román-Manso, L. Garzon, H. R. Gutierrez, M. Terrones, C. Ocal, M.I. Osendi, M. Belmonte, In situ processing of electrically conducting graphene/SiC nanocomposites, J. Eur. Ceram. Soc. 33 (10) (2013) 1665-1674.

[22] B. Román-Manso, Y. Chevillotte, M. I. Osendi, M. Belmonte, P. Miranzo, Thermal conductivity of silicon carbide composites with highly oriented graphene nanoplatelets, J. Eur. Ceram. Soc. 36 (16) (2016) 3987-3993.

[23] P. Miranzo, L. López-Mir, B. Román-Manso, M. Belmonte, M.I. Osendi, C. Ocal, Prominent local transport in silicon carbide composites containing in-situ synthesized three-dimensional graphene networks. J. Eur. Ceram. Soc. 36 (13) (2016), 3073-3081.

[24] S. I. Nakashima, H. Harima, Raman investigation of SiC polytypes, Physica Status Solidi (a) 162(1) (1997), 39-64.

[25] A. C. Ferrari, J. C. Meyer, V. Scardaci, C. Casiraghi, M. Lazzeri, F. Mauri, S. Piscanec, D. Jiang, K. S. Novoselov, S. Roth, A. K. Geim, Raman spectrum of graphene and graphene layers. Phys. Rev. Lett. 97 (2006) 187401-187404.